

5-1-1992

Assessing the Contributions of Surface Waves and Complex Rays to Far-Field Mie Scattering by Use of the Debye Series

Edward A. Hovenac

James A. Lock

Cleveland State University, j.lock@csuohio.edu

Follow this and additional works at: https://engagedscholarship.csuohio.edu/sciphysics_facpub



Part of the [Physics Commons](#)

How does access to this work benefit you? Let us know!

Original Citation

Hovenac, Edward A. and James A. Lock. "Assessing the Contributions of Surface Waves and Complex Rays to Far-Field Mie Scattering by Use of the Debye Series." *Journal of the Optical Society of America A: Optics Image Science and Vision* 9 (1992): 781-795.

Repository Citation

Hovenac, Edward A. and Lock, James A., "Assessing the Contributions of Surface Waves and Complex Rays to Far-Field Mie Scattering by Use of the Debye Series" (1992). *Physics Faculty Publications*. 84.
https://engagedscholarship.csuohio.edu/sciphysics_facpub/84

This Article is brought to you for free and open access by the Physics Department at EngagedScholarship@CSU. It has been accepted for inclusion in Physics Faculty Publications by an authorized administrator of EngagedScholarship@CSU. For more information, please contact library.es@csuohio.edu.

Assessing the contributions of surface waves and complex rays to far-field Mie scattering by use of the Debye series

Edward A. Hovenac

*Sverdrup Technology, Inc., National Aeronautics and Space Administration Lewis Research Center Group,
Cleveland, Ohio 44135*

James A. Lock

Department of Physics, Cleveland State University, Cleveland, Ohio 44115

Received August 6, 1991; revised manuscript received October 30, 1991; accepted November 1, 1991

The contributions of complex rays and the secondary radiation shed by surface waves to scattering by a dielectric sphere are calculated in the context of the Debye-series expansion of the Mie scattering amplitudes. Also, the contributions of geometrical rays are reviewed and compared with those of the Debye series. Interference effects among surface waves, complex rays, and geometrical rays are calculated, and the possibility of observing these interference effects is discussed. Experimental data supporting the observation of a surface-wave-geometrical-ray-interference pattern are presented.

1. INTRODUCTION

The infinite series of transverse-electric (TE) and transverse-magnetic (TM) spherical multipole partial waves, known as the Mie scattering formalism, is an exact solution to the scattering of a linearly polarized plane electromagnetic wave by a dielectric sphere.¹⁻³ Being an exact solution, the Mie infinite series contains all the effects that contribute to the scattering. These effects for the most part are not readily identifiable in the complicated terms of the Mie infinite series. It turns out that writing each term of the Mie infinite series as another infinite series, known as the Debye series, clarifies the physical origins of many effects that occur in electromagnetic scattering.⁴⁻⁹ In ray theory, when a geometrical light ray is incident upon a dielectric sphere it is partially reflected by the sphere surface, partially transmitted through the sphere, and partially transmitted after making an arbitrary number of internal reflections. Analogously, each term of the Debye-series decomposition of an individual TE or TM partial-wave scattering amplitude may be interpreted as diffraction of the corresponding spherical multipole wave or its reflection by the sphere surface ($p = 0$) or as transmission through the sphere ($p = 1$) or transmission after making $p - 1$ internal reflections ($p \geq 2$).

Expressed in this way, the total scattered electric field takes the form of a double sum. One sum is over partial waves, and the other sum is over the number of interactions p that each partial wave makes with the sphere surface before propagating into the far field. For scattering in the short-wavelength limit, the sum over partial waves has long been known to be slowly convergent. But the sum over surface interactions is expected on physical grounds to be rapidly convergent for nearly all partial waves since summing over multiple internal reflections resembles the summing of a geometrical series. The major exception to this rapid convergence is for partial waves

in the edge region, corresponding to geometrical light rays incident upon the sphere at grazing incidence, where the internal reflection coefficient is nearly unity.⁵

For most scattering angles the far-field scattered electric field is dominated by the contributions corresponding to geometrical light rays.¹⁰ Occasionally, however, other mechanisms dominate the scattering. For example, the $p - 1$ -order rainbow caustic occurs at the scattering angle where two light rays coalesce after having made $p - 1$ internal reflections within the dielectric sphere.¹¹ A rainbow separates two regions of scattering in which the numbers of contributing geometrical light rays differ by two. To one side of the rainbow the two $p - 1$ internal reflection rays form an interference pattern known as supernumerary rainbows.¹² Although these two rays are absent on the other side of the rainbow, their contribution to the scattered light does not discontinuously fall to zero at the two-ray-zero-ray transition. Rather, their contribution smoothly but rapidly decreases owing to their metamorphosis into a complex ray in the zero-geometrical-ray region.¹³⁻¹⁵

Another example in which the scattering is dominated by effects other than geometrical light rays occurs when light is incident upon the sphere at grazing incidence. Beyond the scattering angle of the grazing-incidence ray, the contribution of this ray to the scattered intensity again does not discontinuously fall to zero at the one-ray-zero-ray transition. This is due to the creation of electromagnetic surface waves at the point of grazing incidence upon the sphere.^{5-7,16,17} These waves travel along the sphere circumference, and, while doing so, they shed secondary radiation that propagates into the far field. This secondary radiation produces radiation damping of the surface waves. As a result, the surface-wave amplitude dies off exponentially along the sphere's circumference, and the amplitude of the secondary radiation propagating into the far field dies off exponentially as a function of the

scattering angle. The far-field intensity produced by the surface waves joins smoothly with the far-field intensity produced by the geometrical light rays in the vicinity of the one-ray-zero-ray transition. This smooth intensity transition is known as the Fock transition.^{5-7,18}

A question of interest is whether, under favorable circumstances, some of these nongeometrical mechanisms that weakly contribute to the scattering, namely, surface waves and complex rays, may be observed. It has been known for some time that the optical glory is dominated by the contribution of $p = 2$ surface waves.^{7,15,19,20} In addition, a subtle effect of the complex ray in the neighborhood of a transverse cusp caustic has been predicted²¹⁻²⁴ and tentatively observed.²⁵ One of our purposes is to assess the practicality of additional observations of surface waves and complex rays in light scattering by a dielectric sphere. The observations that we examine employ the interference of surface waves or complex rays with geometrical light rays. The technique of observing relatively weak contributions to scattering by their interference with more dominant contributions has long been employed in quantum-mechanical scattering.²⁶ We believe that this method was not previously considered for surface waves or complex rays in the context of light scattering by a dielectric sphere.

This paper has a second and more theoretical purpose as well. Although light-scattering experiments measure the full scattered intensity rather than only one Debye-series component at a time, the Debye-series decomposition of the scattering amplitudes is a powerful tool for understanding the physical mechanisms that produce the scattering. The individual Debye-component intensities allow one to examine a single scattering mechanism in isolation from all the other mechanisms that either dominate it or otherwise obscure its effects. The Debye-series-component intensities are found to exhibit a number of novel features and interference structures that are not evident in the total Mie intensity. Even though many of these novel structures may not be observable in practice, we believe that determining their physical origins increases our fundamental understanding of the scattering process.

The remainder of this paper is organized as follows. In Section 2 we review the contribution of geometrical light rays to the scattered intensity. In Section 3 we review the Airy theory of the $p - 1$ -order rainbow and compare its accuracy with that of the p term of the Debye-series expansion of the scattered intensity. We parameterize the complex ray in the zero-ray region adjacent to the rainbow in terms of the Airy integral. In Section 4 we review the complex-angular-momentum parameterization of surface waves and compare its accuracy with that of the $p = 1$ (i.e., transmission) term of the Debye series. Next, in Sections 5-7, using these models for complex rays, surface waves, and geometrical light rays, we examine the interference between (1) surface waves and geometrical rays, (2) complex rays and geometrical rays, and (3) surface waves and complex rays that occur in the various Debye-series-component intensities. In Section 8 we describe an experiment in which we observed the surface-wave-geometrical-ray interference. Finally, we present our conclusions in Section 9.

2. GEOMETRICAL LIGHT RAYS

Consider a linearly polarized geometrical light ray with field strength E_0 and wavelength λ incident with the angle θ_i upon a dielectric sphere of radius a and refractive index n as in Fig. 1. The size parameter of the sphere is defined as

$$x = \frac{2\pi a}{\lambda}. \quad (1)$$

The angle of deflection of the geometrical ray as it leaves the sphere after having made $p - 1$ internal reflections is

$$\Theta = (p - 1)\pi + 2\theta_i - 2p\theta_r, \quad (2)$$

where

$$\sin \theta_i = n \sin \theta_r. \quad (3)$$

The scattering angle corresponding to this deflection is

$$\theta = \begin{cases} \Theta - 2\pi N & \text{if } 2\pi N \leq \Theta \leq 2\pi(N + 1/2) \\ 2\pi(N + 1) - \Theta & \text{if } 2\pi(N + 1/2) < \Theta \leq 2\pi(N + 1) \end{cases}, \quad (4)$$

where N is an integer. This relation confines the scattering angle to the interval $0 \leq \theta \leq 180^\circ$. The fraction of the geometrical ray's incident TE or TM polarized electric field that is transmitted from the exterior to the interior of the sphere is $T^{21}(\theta_i)$, the fraction that is internally reflected is $R^{11}(\theta_i)$, and the fraction that is transmitted from the interior to the exterior is $T^{12}(\theta_i)$. The superscript 1 denotes the region inside the sphere, and the superscript 2 denotes the region outside the sphere. When $x \gg 1$, these fractions are approximated by the Fresnel coefficients for oblique incidence upon a flat interface with either the TE or the TM polarization.²⁷

The optical path length of the ray from the entrance plane of the sphere to the exit plane is

$$L = 2a(pn \cos \theta_r - \cos \theta_i) + 2a. \quad (5)$$

The electric field of the ray scattered in the θ direction

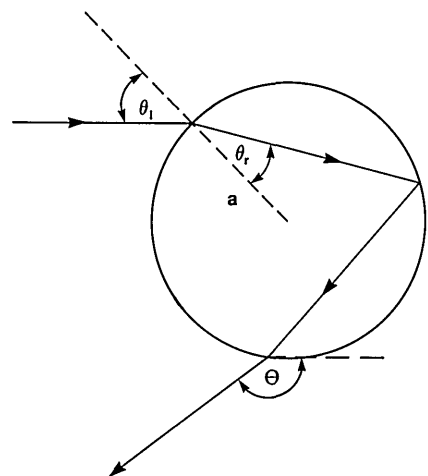


Fig. 1. Deflection of a geometrical light ray through the angle Θ by a dielectric sphere of radius a and refractive index n .

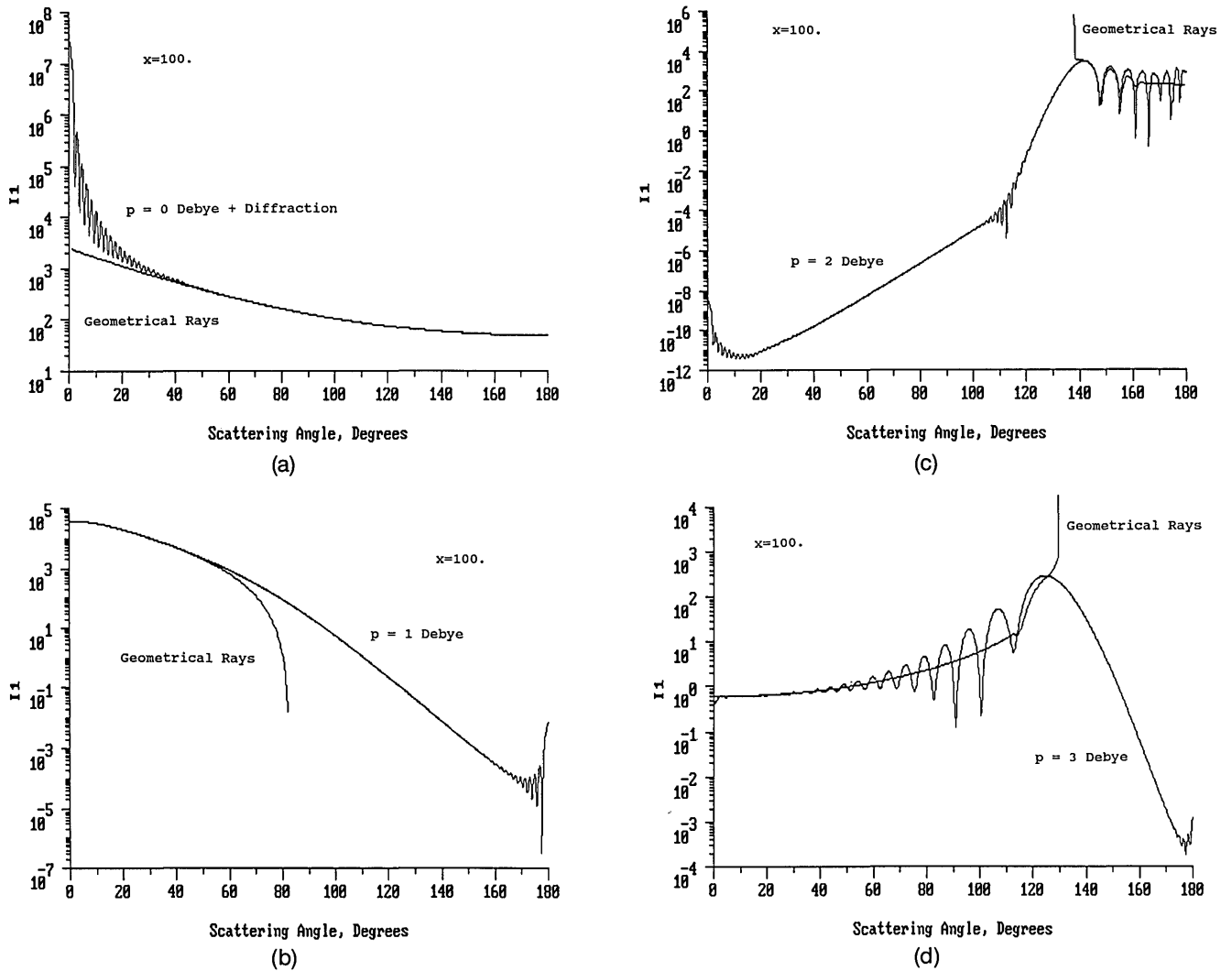


Fig. 2. Comparison of the p -term Debye-series-component intensity I_1 with the prediction of geometrical optics, Eq. (6), for all the contributing TE polarized ray trajectories for $x = 100$ and $n = 1.333$. (a) Debye $p = 0$ plus diffraction compared with the reflected geometrical rays; (b) Debye $p = 1$ compared with the transmitted geometrical rays; (c) Debye $p = 2$ compared with the single-internal-reflection geometrical rays; (d) Debye $p = 3$ compared with the two internal reflection geometrical rays.

after $p - 1$ internal reflections is then¹¹

$$E_{\text{geometrical ray}}^p(\theta) = \frac{E_0 a}{R} \left[\frac{\sin \theta_i \cos \theta_i}{2 \sin \theta \left| 1 - \frac{p \cos \theta_i}{n \cos \theta_r} \right|} \right]^{1/2} T^{21}(\theta_i) \times [R^{11}(\theta_i)]^{p-1} T^{12}(\theta_i) \exp(ikR) \exp(2\pi i L/\lambda) \exp(i\zeta) \quad (6)$$

for either polarization state, where R is the distance from the center of the sphere to the observer and ζ is a phase factor that contains the effect of the ray trajectory crossing focal lines.²⁸ For almost all values of p , there are a number of values of θ_i that give rise to the same scattering angle θ . As a result, when Eq. (6) is used in obtaining the total ray optics scattered electric field, all the contributing ray trajectories for the scattering angle θ must be summed.

As mentioned above, the far-field Mie scattered electric field at most angles is dominated by the contributions of geometrical light rays. A comparison between the geometrical-ray model and the various Debye-series-

component intensities can be used to map the angular regions corresponding to the various p terms that are dominated by the geometrical light rays and the angular regions that are dominated by other effects. The appropriate formulas for the various terms of the Debye-series expansion of the scattered electric field and their relation to the TE and the TM polarization states of the geometrical rays are given in Appendix A.

Figures 2(a), 2(b), 2(c), and 2(d) show the comparison between the Debye scattered intensities ($I_1 \equiv |S_1|^2$) and the corresponding TE polarization state of the geometrical ray for $p = 0, 1, 2$, and 3 , respectively, for a sphere with $x = 100$ and $n = 1.333$. Note that in Fig. 2(a) the Debye-series plot for $p = 0$ also includes the diffraction term. Details describing the necessity of combining the $p = 0$ (reflection) term with the diffraction term are given in Appendix A. Also note from Fig. 2(a) that agreement between the geometrical-ray model of reflection and the Debye $p = 0$ plus diffraction intensity is excellent for the larger scattering angles at which the reflection term of the Debye series dominates. Thus ray optics is a good

model for reflection from a sphere with size parameters as low as 100 or less.²⁹

Figure 2(b) compares the geometrical-ray model of the transmitted light with the $p = 1$ term of the Debye series. The ray optics model predicts that no light is scattered past $\theta = 82.79^\circ$, whereas the intensity contributed by the $p = 1$ term of the Debye series continues out to 180° . This continuation is produced by the secondary radiation shed by surface waves and is addressed in more detail in Section 4. One other point of interest is the oscillations near $\theta = 180^\circ$ in the Debye-series-component intensity. This is the interference pattern that surrounds the back-scatter glory axial caustic.³⁰⁻³²

Figures 2(c) and 2(d) compare the geometrical-ray models of the light making one and two internal reflections with the $p = 2$ and the $p = 3$ terms of the Debye series. In both cases ray optics predicts large angular intervals in which no rays are scattered and an infinite intensity at the positions of the rainbows. In contrast, the Debye-series-component intensities extend over all the scattering angles and show a broad increase near the rainbow, with the characteristic supernumeraries located to one side. Also note from Fig. 2(c) the oscillations in the intensity near $\theta = 0^\circ$ for the $p = 2$ Debye contribution. This is the interference pattern that surrounds the forward glory axial caustic.^{26,33}

3. AIRY THEORY OF THE RAINBOW

As is seen in Figs. 2(c) and 2(d), the electric field of Eq. (6) for the geometrical rays that have made $p - 1$ internal reflections incorrectly predicts an infinite intensity in the direction of the rainbow scattering angle θ^R . This angle is given by Eq. (4) with

$$\Theta^R = (p - 1)\pi + 2\theta_i^R - 2p\theta_r^R, \quad (7)$$

$$\cos^2 \theta_i^R = \frac{n^2 - 1}{p^2 - 1}. \quad (8)$$

In Airy theory, the shape of the wave front leaving the dielectric sphere in the vicinity of θ^R is cubic to a first approximation.³⁴ If this exiting wave front is then Fraunhofer diffracted into the far field, the TE or the TM polarized electric field in the vicinity of θ^R becomes³⁵

$$\begin{aligned} E_{\text{Airy}}^p(\theta) &= \frac{E_0 a \exp(ikR)}{R} \left(\frac{2\pi \sin \theta_i^R}{\sin \theta^R} \right)^{1/2} \frac{x^{1/6}}{h^{1/3}} T^{21}(\theta_i^R) \\ &\times [R^{11}(\theta_i^R)]^{p-1} T^{12}(\theta_i^R) \times \text{Ai} \left(\frac{-x^{2/3} \Delta}{h^{1/3}} \right) \\ &\times \exp(2\pi i L^R / \lambda) \exp \left[(ix\Delta) \left(\frac{p^2 - n^2}{p^2 - 1} \right)^{1/2} \right], \end{aligned} \quad (9)$$

where

$$\Delta = \theta - \theta^R, \quad (10)$$

$$h = \frac{(p^2 - 1)^2 (p^2 - n^2)^{1/2}}{p^2 (n^2 - 1)^{3/2}}, \quad (11)$$

L^R is Eq. (5) evaluated at the rainbow angle, and Ai is the Airy integral.³⁶ For negative values of its argument, the Airy integral is oscillatory and describes the supernumerary interference pattern in the two-geometrical-ray region. For positive values of its argument, the Airy integral rap-

idly dies off in the zero-geometrical-ray region as

$$\text{Ai}(u) \approx \frac{1}{2\pi^{1/2}} \left(\frac{2}{3} u^{3/2} \right)^{-1/4} \exp \left(-\frac{2}{3} u^{3/2} \right) \quad (12)$$

for $u \gg 1$.

In the complex-angular-momentum analysis of the Debye-series terms, for a given value of p , we convert the sum over partial waves into an integral over an effective impact parameter (i.e., how far off center an incident ray strikes the sphere) by using the modified Watson transformation.⁵⁻⁷ The numerical value of this integral is dominated in the small-wavelength limit by the regions of stationary phase and residue poles of the integrand. The stationary-phase regions produce contributions to the integral that resemble the effects of geometrical light rays. This result is the motivation for the localization principle mentioned below in Section 4. The residue pole contributions correspond to the shedding of secondary radiation by surface waves.

After the two geometrical rays coalesce at the rainbow scattering angle, if the scattering angle is further decreased the impact parameters of the two rays in the complex-angular-momentum analysis leave the real axis and migrate into the complex plane. The contribution to the Debye-term integral from these complex impact-parameter stationary-phase points is known as the complex ray contribution to the scattering.

The complex ray is loosely analogous to an exponentially damped wave or an evanescent wave. When a plane wave is incident upon a flat dielectric interface, a portion of the wave is refracted through the interface at an angle θ_r as determined by Snell's law [$\theta_r = \arcsin(n_i/n_r \sin \theta_i)$]. If the wave is incident from a denser medium (i.e., $n_i/n_r > 1$) and the angle of incidence θ_i of the wave increases past the critical angle for total internal reflection (i.e., $n_i/n_r \sin \theta_i > 1$), then θ_r must become complex to satisfy Snell's law. Thus the angle of refraction leaves the real axis and migrates into the complex plane, and an evanescent wave is formed. The imaginary part of the angle of refraction is responsible for the damping of the evanescent wave.

Since the zeroth-order approximation to the complex-angular-momentum analysis gives results identical to those of Airy theory, we take the rapid falloff of the Airy integral for $u \gg 1$ as our parameterization of the scattering produced by the complex ray.

The intensity of the $p - 1$ -order rainbow in Airy theory,

$$I_{\text{Airy}}^p(\theta) = |E_{\text{Airy}}^p(\theta)|^2, \quad (13)$$

was previously compared with the full Mie intensity for $x \sim 15,000$ for only the first- and the second-order rainbows ($p = 2, 3$).³⁵ The reason that comparisons for higher-order rainbows were not previously made is that the Mie intensity is dominated by the much larger diffracted, reflected, and transmitted contributions in the regions where these rainbows occur. Only in Alexander's dark band between the first- and the second-order rainbows is the background intensity low enough that the features of the fifth- and the sixth-order rainbows may be qualitatively examined by using Airy theory.^{35,37,38} However, if $I_{\text{Airy}}^p(\theta)$ were compared with the intensity

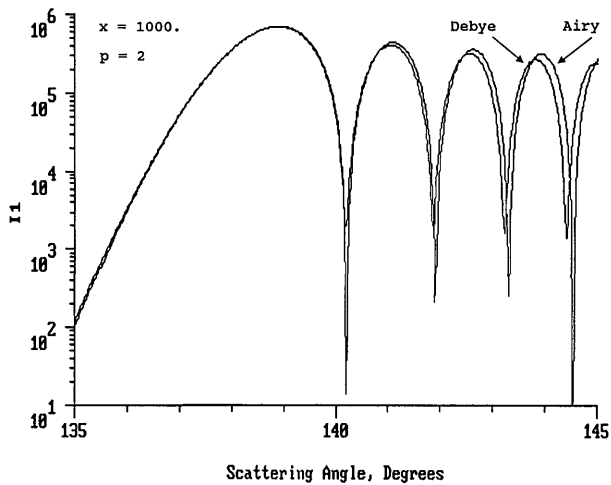


Fig. 3. Comparison of the $p = 2$ Debye-component intensity I_1 with the Airy theory approximation of Eq. (13) for the TE polarization state, $x = 1000$, and $n = 1.333$.

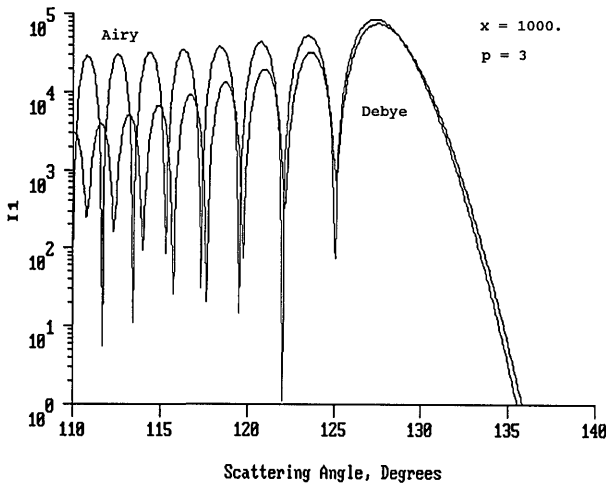


Fig. 4. Comparison of the $p = 3$ Debye-component intensity I_1 with the Airy theory approximation of Eq. (13) for the TE polarization state, $x = 1000$, and $n = 1.333$.

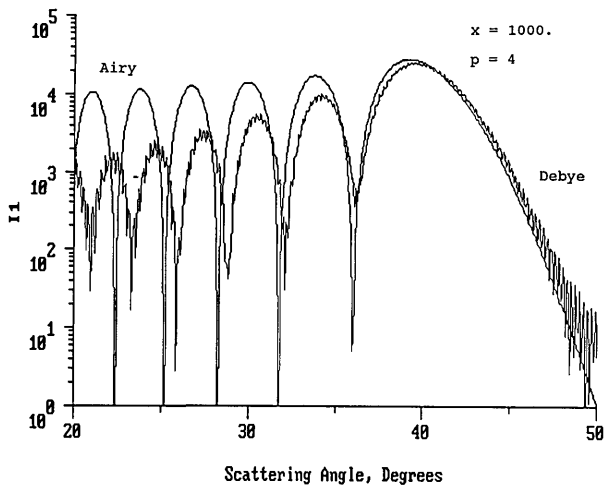


Fig. 5. Comparison of the $p = 4$ Debye-component intensity I_1 with the Airy theory approximation of Eq. (13) for the TE polarization state, $x = 1000$, and $n = 1.333$.

corresponding to only the p term of the Debye-series expansion of the Mie scattering amplitudes, the other contributions to the Mie amplitudes that would normally

obscure the relatively weak high-order rainbows would be removed from consideration. In the remainder of this section we use the Debye-term comparison to provide a sensitive test of the validity of Airy theory for high-order rainbows.

Using Eqs. (9) and (13) and the results of Appendix A, we give the comparisons between Airy theory and the Debye-series terms for the first- through the fifth-order rainbows in Figs. 3–7 for $x = 1000$ and $n = 1.333$ for the dominant polarization [i.e., for the Debye scattering intensity $I_1(\theta)$ and the TE polarization for Airy theory].

The Airy theory formula of Eq. (9) neglects the variations in the Fresnel reflection and transmission coefficients as a function of θ_i in the vicinity of θ_i^R . This variation is relatively unimportant for the primary rainbow in the dominant polarization, as is seen in Fig. 3. But, as is evidenced by Figs. 4–7, the variation in the Fresnel coefficients is important for all higher-order rainbows since θ_i^R is closer to $\pi/2$, where the transmission and the reflection Fresnel coefficients are rapidly increasing or decreasing functions of θ_i . This variation is also important in the nondominant polarization [i.e., for the De-

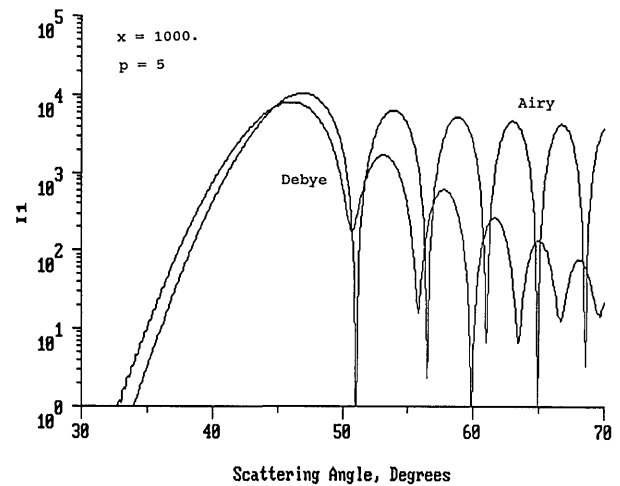


Fig. 6. Comparison of the $p = 5$ Debye-component intensity I_1 with the Airy theory approximation of Eq. (13) for the TE polarization state, $x = 1000$, and $n = 1.333$.

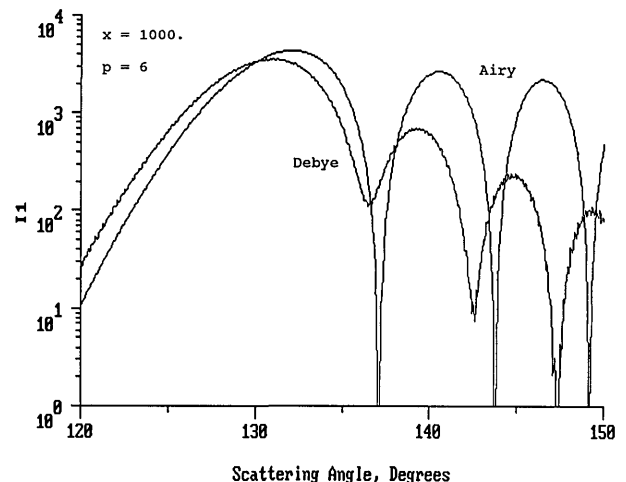


Fig. 7. Comparison of the $p = 6$ Debye-component intensity I_1 with the Airy theory approximation of Eq. (13) for the TE polarization state, $x = 1000$, and $n = 1.333$.

bye scattering intensity $I_2(\theta)$ and the TM polarization for Airy theory] since θ_i^R is near the Brewster angle for this polarization and the internal reflection of the contributing rays is weak.³⁹ For large droplets with $x \approx 20,000$ for the $p - 1$ -order rainbow in the dominant polarization, the Airy theory approximation of Eq. (13) was found to be virtually identical near the primary maximum to the exact Debye-series calculation for all the values of p that were examined.

4. SURFACE WAVES

For $x \gg 1$, the localization principle⁴⁰ associates a small number of spherical multipole partial waves centered about the partial-wave number l_{ave} with a geometrical light ray whose angle of incidence on the sphere is

$$\sin \theta_i \approx \frac{l_{\text{ave}}}{x}. \quad (14)$$

For example, small values of l correspond to rays incident near the center line of the sphere, and values of $l \sim x$ correspond to light rays incident upon the sphere at grazing incidence. In ray theory such a grazing ray is entirely reflected by the sphere. In wave theory the grazing incidence also creates surface waves that propagate along the circumference of the sphere. At every point along the circumference they shed secondary radiation tangentially, which then propagates into the far zone. Some of the surface waves also refract into the sphere. The angle of the refracted wave inside the sphere is given by Snell's law. This angle turns out to be the critical angle because the incident wave (i.e., the surface wave) is propagating parallel to the surface. After the refracted wave propagates across the interior of the sphere and reaches the opposite side, it is again refracted at the surface. Since the angle that the refracted wave makes with the surface is again the critical angle, the wave exits the sphere parallel to the surface and forms another surface wave. Thus a portion of the original surface wave takes a shortcut through the sphere before returning to the surface to shed more secondary radiation tangentially into the far zone.^{5,6,18}

The phenomenon of surface waves has long been known and has many applications in electromagnetism,^{13,41} acoustics,⁴² and quantum-mechanical scattering.⁴³ It is only comparatively recently,⁷ however, that the scattering amplitude for electromagnetic surface waves on a dielectric sphere has been calculated. In this section we review these results and compare them with the results of Debye-series calculations.

The surface waves, otherwise known as creeping waves or surface guided modes, resemble electromagnetic fields propagating in a leaky waveguide duct on the exterior of the sphere.⁴⁴ The energy that leaks out of the effective waveguide duct into the sphere is the above-mentioned shortcut through the sphere. The energy that leaks outward from the sphere surface and propagates into the far field is the shed secondary radiation described in this section. We consider the surface wave in the j waveguide mode, where $j \geq 1$ is an integer, that takes p shortcuts through the sphere and thereby makes $p - 1$ internal reflections. Such a surface wave is pictorially represented in Fig. 8. Let ξ be the total angle traveled by the

surface wave on the circumference of the sphere. The distance

$$T = \frac{2a}{n}(n^2 - 1)^{1/2} \quad (15)$$

is the length of a shortcut through the sphere made at the critical refraction angle θ_r^C , given by

$$\sin \theta_r^C = \frac{1}{n}. \quad (16)$$

The wave vector of the surface wave during the shortcut is

$$k_{\text{shortcut}} = nk, \quad (17)$$

and the wave vector as it propagates along the circumference is⁷

$$k_{\text{surface}}^j = k + \frac{X_j}{2a} \left(\frac{x}{2} \right)^{1/3} + i \left[\frac{3^{1/2} X_j}{2a} \left(\frac{x}{2} \right)^{1/3} - \frac{\kappa}{a} (n^2 - 1)^{1/2} \right], \quad (18)$$

where X_j is defined by

$$Ai(-X_j) = 0 \quad (19)$$

and

$$\kappa = \begin{cases} 1 & \text{for the } S_1 \text{ scattering amplitude} \\ n^2 & \text{for the } S_2 \text{ scattering amplitude} \end{cases} \quad (20)$$

The real part of k_{surface}^j indicates that the propagation speed of the surface wave along the circumference is less than C . The imaginary part describes the radiation damping. The scattered electric field that is due to the secondary radiation produced by the j mode of the $p - 1$ internal reflection surface wave is⁷

$$E_{\text{surface wave}}^{p,j}(\theta) = \frac{E_0 a \exp(ikR)}{R(\sin \theta)^{1/2}} \frac{\exp(i\pi/12)}{2\pi^{1/2} a_j^{1/2}} \left(\frac{2}{x} \right)^{1/6} \times \exp(ipk_{\text{shortcut}} T) \exp(ik_{\text{surface}}^j a \xi) \exp(2ika) \times \sum_{m=1}^p \frac{(p-1)!}{(m-1)!(p-m)!} \left[\frac{2\kappa}{(n^2 - 1)^{1/2}} \right]^m \frac{\xi^m}{m!}, \quad (21)$$

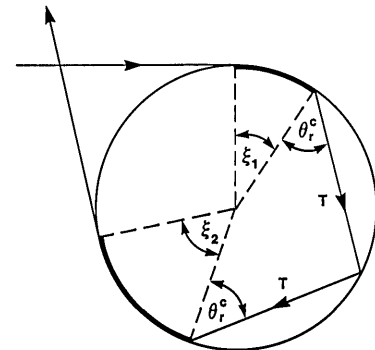


Fig. 8. Secondary radiation shed into the far field by a $p = 2$ surface wave that travels the angular distance $\xi = \xi_1 + \xi_2$ along the circumference of the sphere. The path segments marked T denote the shortcuts made by the surface wave through the sphere, and the thick arc segments denote propagation along the sphere surface.

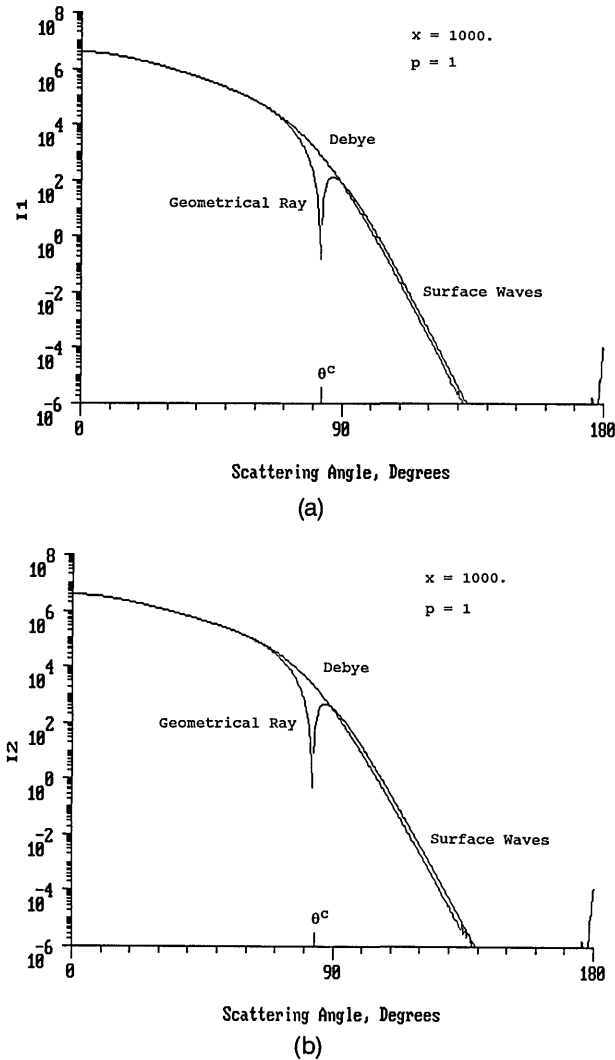


Fig. 9. Comparison of the $p = 1$ Debye-component intensity with the transmitted geometrical-ray and surface-wave contributions of Eqs. (6) and (21) for $x = 1000$ and $n = 1.333$. (a) The I_1 Debye scattered intensity, the TE polarized ray, and the TE polarized surface wave; (b) the I_2 Debye scattered intensity, the TM polarized ray, and the TM polarized surface wave.

where a_j' is defined in terms of the derivative of the Airy integral by

$$Ai'(-X_j) = a_j' \quad (22)$$

and the relationship between the scattering angle and the angle ξ along the circumference is given by Eq. (4) with

$$\Theta = p\pi - 2p\theta_r^C + \xi. \quad (23)$$

The associated scattered intensity for either the S_1 or the S_2 scattering amplitude is

$$I_{\text{surface wave}}^p(\theta) = \left| \sum_{j=1}^{\infty} E_{\text{surface wave}}^{p,j}(\theta) \right|^2. \quad (24)$$

In practice, only the $j = 1$ term of this sum is usually considered. This corresponds to the largest-amplitude surface wave and the strongest secondary radiation in the far field.

The accuracy of the surface wave parameterization of Eq. (21) was tested by comparing the scattered intensities

owing to the TE and the TM polarized $p = 1$ geometrical rays plus their corresponding $p = 1, j = 1$ surface waves with the intensity of the $p = 1$ term of the Debye series for the S_1 and the S_2 scattering amplitudes, respectively. Figure 9 shows the results for both polarization states for $x = 1000$ and $n = 1.333$. In the vicinity of the critical scattering angle, a complete comparison would require that Eqs. (6) and (21) be replaced by the Fock transition formulas of Refs. 5–7 that smoothly connect the ray theory intensity below the critical scattering angle with the surface-wave intensity above the critical scattering angle. As x increases, the surface-wave encroachment of the scattered intensity into the scattering angle region $\theta > \theta^C$ decreases.

5. SURFACE-WAVE-GEOMETRICAL-RAY INTERFERENCE

Consider the vicinity of the $p - 1$ -order rainbow. In ray theory the geometrical light ray that is incident upon the sphere with the angle θ_i^R exits at the rainbow scattering angle θ^R . The two rays that exit in the direction $\theta > \theta^R$ and interfere to produce the supernumerary pattern are incident upon the sphere with the angles $\theta_i < \theta_i^R$ and $\theta_i > \theta_i^R$. As one progresses farther into the supernumerary region, the angles of incidence of the contributing rays continue to decrease and to increase, respectively, until the one with the larger incident angle approaches $\theta_i = \pi/2$. In ray theory the supernumerary interference pattern ends at $\theta_i = \pi/2$. This corresponds to the scattering angle θ^C given by Eq. (4) with

$$\Theta^C = p\pi - 2p\theta_r^C. \quad (25)$$

For scattering angles beyond θ^C only a single remaining geometrical ray, the one with $\theta_i < \theta_i^R$, contributes to the scattered intensity. In wave theory, however, the grazing-incidence geometrical ray launches surface waves. For $\theta > \theta^C$ the remaining geometrical ray and the secondary radiation shed by the surface waves continue to interfere, thereby extending the supernumerary region beyond the ray theory limit. This surface-wave-geometrical-ray interference is indicated pictorially in Fig. 10.

For the first-order rainbow with $n = 1.333$, the supernumerary region begins at $\theta^R = 137.92^\circ$ and ends at

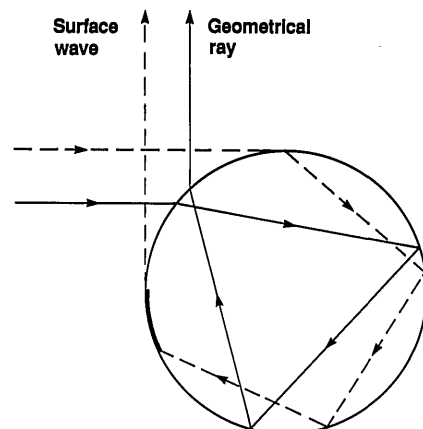


Fig. 10. A $p = 3$ geometrical ray (solid line) and a $p = 3$ surface wave (dashed line) that interfere in the far field.

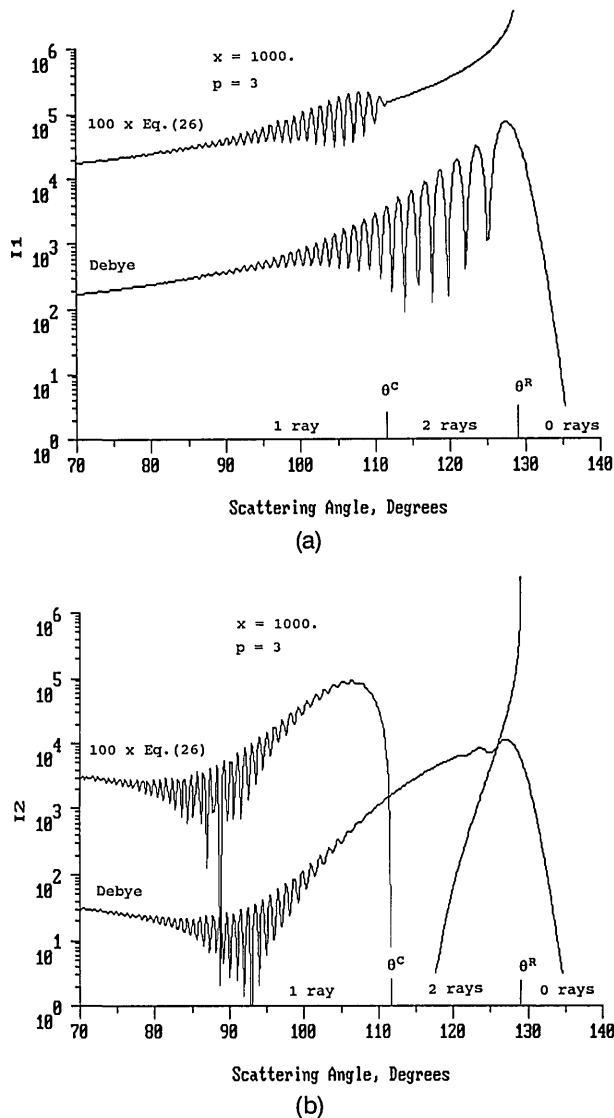


Fig. 11. Comparison of the $p = 3$ Debye-component intensity with the approximation of Eq. (26) for $x = 1000$ and $n = 1.333$. The approximation of Eq. (26) has been offset by a factor of 100 for clarity. (a) The I_1 Debye scattered intensity, the TE polarized ray, and the TE polarized surface wave; (b) the I_2 Debye scattered amplitude, the TM polarized ray, and the TM polarized surface wave.

$\theta^C = 165.57^\circ$ according to ray theory. The interference of the $p = 2$ surface waves with the remaining $p = 2$ geometrical ray having $\theta_i < 14.6^\circ$ encroaches into the glory region and is not easily observed because of its interference with other backscattering mechanisms. For the third-order rainbow the supernumerary region begins at $\theta^R = 41.74^\circ$ and ends at $\theta^C = 28.86^\circ$ according to ray theory. The interference between the $p = 4$ surface waves and the remaining $p = 4$ geometrical ray having $\theta_i < 62.6^\circ$ encroaches into the forward diffraction region and is again not easily observed because of the dominance of other forward-scattering mechanisms. For the second-order rainbow, however, the effect may be amenable to observation. For $p = 3$ the supernumerary region begins at $\theta^R = 129.11^\circ$ and ends at $\theta^C = 111.64^\circ$ according to ray theory. The surface-wave-geometrical-ray interference propagates toward $\theta = 90^\circ$, where the total Mie intensity and thus the strength of the competing scattering

mechanisms are generally low, and the effect might be observable.

To see how the interference is imprinted on the scattered intensity, we compare in Fig. 11 the $p = 3$ term of the Debye series for each polarization with

$$I_{\text{approximate}}^{p=3}(\theta) = |E_{\text{geometrical ray}}^{p=3}(\theta) + E_{\text{surface wave}}^{p=3,j=1}(\theta)|^2, \quad (26)$$

using only one of the geometrical rays that contribute to the second-order rainbow, the one incident closer to the center line of the sphere. In this figure Eq. (26) has been offset by a factor of 100 for clarity. As mentioned above, the contribution of the geometrical ray becomes infinite at the rainbow angle. This is apparent in Fig. 11. The Debye-series-component intensity in Fig. 11 shows an oscillatory structure for both polarizations that extends well below θ^C . This is the surface-wave-geometrical-ray interference. The approximation of Eq. (26) agrees well with the Debye-series result for $\theta \ll \theta^C$ both in the amplitude and in the period of the oscillation. Near θ^C the comparison is poor because Eq. (26) should be replaced by the above-mentioned Fock transition formulas at the geometrical-ray-surface-wave transition.⁵ The falloff in the amplitude of the oscillatory structure of the Debye $p = 3$ intensity near θ^C for the dominant polarization (i.e., the S_1 amplitude) could even be used to measure the Fock transition effect experimentally. In Fig. 11(b) the vanishing of the Fresnel reflection coefficient of the geometrical ray at the Brewster angle ($\theta_i^B = 53.12^\circ$, $\theta^B = 115.02^\circ$) is also evident.

A feature of Fig. 11(b) that was unanticipated is the virtual nonexistence of supernumeraries for the second-order rainbow in the nondominant polarization (i.e., the S_2 amplitude) for $x \sim 1000$. For very large spheres (i.e., $x \sim 20,000$) they do appear but are quite weak compared with the supernumeraries for the dominant polarization. This near absence of nondominant polarization supernumeraries was found for all the rainbows that we examined (the second order through the fifth order) and seems not to have been commented on before. The absence of the supernumeraries is due to the fact that the Brewster angle for the TM polarization is within or near the range of angles θ_i of the supernumerary ray incident closer to the center line of the sphere. The Fresnel reflection coefficient term $[R^{11}]^{p-1}$ of this ray is near zero in much or all of the supernumerary region. Thus the ray has a small amplitude, and its interference with the other supernumerary ray is quite weak.

For a plane wave incident upon a spherical water droplet in the TE polarization state, the intensity of the surface-wave-geometrical-ray interference is approximately 1 order of magnitude weaker than the intensity that is due to reflection by the droplet surface. For the TM polarization state, it is approximately 2 orders of magnitude weaker than the reflection component. As a result, it seems that the surface-wave-geometrical-ray interference of Fig. 11 should not be observable. However, a possibility of observation exists in two different experimental situations. First, it has been found that the intensity of the second-order rainbow for a prolate spheroidal water droplet is enhanced with respect to its intensity for a spherical droplet.³⁸ This relative enhancement may render the surface-wave-geometrical-ray intensity compa-

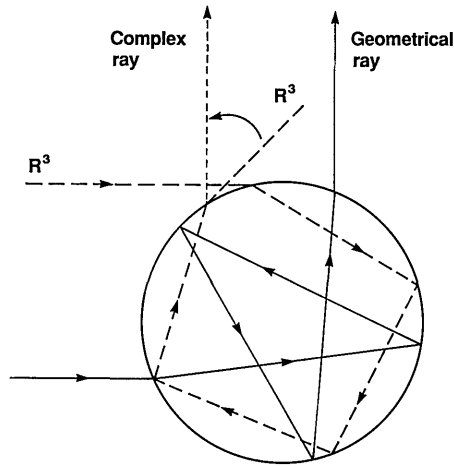


Fig. 12. A $p = 4$ geometrical ray (solid line) and the $p = 4$ complex ray (short-dashed line) that interfere in the far field. The long-dashed line marked R^3 is the third-order rainbow ray. The complex ray occurs for scattering angles larger than that of the rainbow ray.

able with the reflection intensity. Second, if a water droplet is illuminated by a laser beam whose diameter is smaller than the droplet diameter, shifting the beam off center increases the intensity of the second-order rainbow with respect to the competing reflected light.¹² For example, consider the scattered light at the angle at which geometrical optics predicts the end of the supernumerary region (i.e., at $\theta^C = 111.64^\circ$). The contributing supernumerary rays are incident upon the droplet at distances of $0.76a$ and $1.00a$ from the center line of the droplet, while the rays that are reflected from the droplet are incident somewhat closer to the center line of the droplet at a distance of $0.56a$. If the center of an incident laser beam is positioned near the edge of a water droplet, the rays that produce the second-order rainbow will have greater intensity than the rays that are reflected at that angle. We investigate this technique experimentally in Section 8.

6. COMPLEX-RAY-GEOMETRICAL-RAY INTERFERENCE

Consider light rays that make three internal reflections (i.e., $p = 4$ rays) within the sphere, as in Fig. 12. The scattering angle of the third-order rainbow is $\theta^R = 41.74^\circ$, and in ray optics the supernumeraries occur for scattering angles between θ^R and $\theta^C = 28.86^\circ$. The complex ray contributes to the $p = 4$ intensity for $\theta > \theta^R$. In addition, a third geometrical light ray that enters on the opposite side of the center line with $\theta_i \leq 35^\circ$ and makes three internal reflections also exits at $\theta > \theta^R$ and interferes with the complex ray, as in Fig. 12.

The intensity corresponding to the S_1 scattering amplitude $p = 4$ term of the Debye series, shown in Fig. 13, exhibits the third-order rainbow, a few broad supernumeraries for $\theta < \theta^R$, and a much finer oscillatory structure for $\theta > \theta^R$. The amplitude of the finer oscillatory structure grows with increasing θ until the scattering angle is approximately 52° . Thereafter the amplitude decreases. Such behavior is consistent with the interference between the $p = 4$ complex ray and the above-mentioned third $p = 4$ geometrical ray, with the complex ray dominating

for $\theta \leq 52^\circ$ and the geometrical ray dominating for $\theta \geq 52^\circ$. To verify this, we compared the $p = 4$ Debye-series intensity with

$$I_{\text{approximate}}^{p=4}(\theta) = |E_{\text{third geometrical ray}}^{p=4}(\theta) + E_{\text{Airy}}^{p=4}(\theta)|^2 \quad (27)$$

in Fig. 13. Again, the comparison of the amplitude and the period of the oscillatory structure is quite good.

As to the potential observability of this effect, for scattering by a sphere in this angular region the scattering is dominated by transmission and reflection. Although the third-order rainbow from a prolate spheroidal water droplet has been tentatively observed,³⁸ the complex ray-geometrical ray interference pattern of Fig. 13 is more than 3 orders of magnitude weaker than the rainbow maximum. Further, the two rays that contribute to this interference pattern enter on opposite sides of the droplet, and the dominant $p = 0$ reflected ray is incident upon the sphere at virtually the same location where the third-order rainbow ray enters. This renders the off-center laser beam technique ineffective in this situation. Possibly the only hope for the observation of the complex-ray-geometrical-ray interference would be to use the TM polarization state, in which the intensity of the reflected ray falls by more than 1 order of magnitude while the intensity of the third-order rainbow falls by a factor of approximately 4.

7. SURFACE-WAVE-COMPLEX-RAY INTERFERENCE

Since no geometrical light rays make one internal reflection within the sphere and exit with a scattering angle less than $\theta^R = 137.92^\circ$, the $p = 2$ term of the Debye series should be a near-ideal situation in which to examine numerically weak-scattering mechanisms in the region $\theta < \theta^R$. Near the first-order rainbow the $p = 2$ intensity is dominated by the complex ray that falls off faster than exponentially as a function of θ . Since the intensity of the secondary radiation shed by surface waves falls off exponentially as a function of θ , it was previously noted that the scattered intensity that is due to surface waves pro-

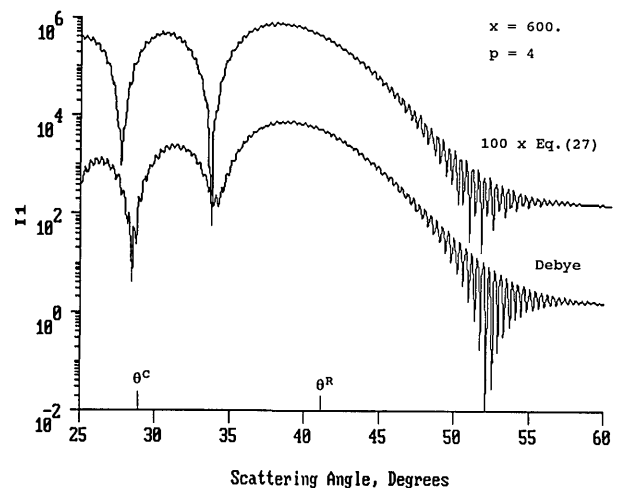


Fig. 13. Comparison of the $p = 4$ Debye-component intensity I_1 with the approximation of Eq. (27) for the TE polarization state and for $x = 600$ and $n = 1.333$. The approximation of Eq. (27) has been offset by a factor of 100 for clarity.

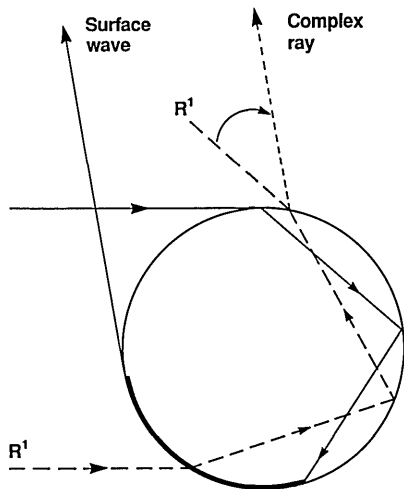


Fig. 14. A $p = 2$ surface wave (solid line) and the $p = 2$ complex ray (short-dashed line) that interfere in the far field. The long-dashed line marked R^1 is the first-order rainbow ray. The complex ray occurs for scattering angles smaller than that of the rainbow ray.

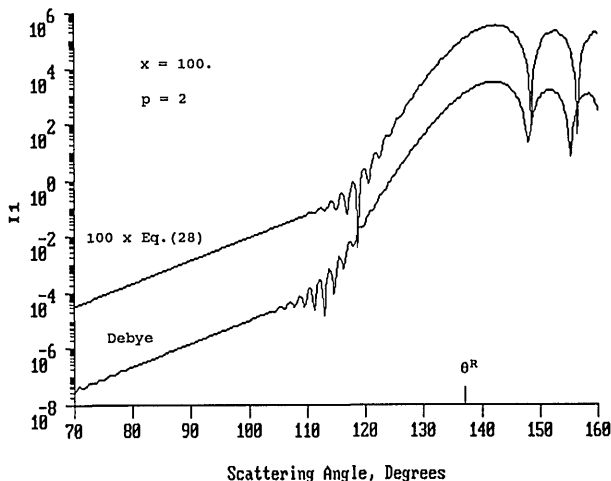


Fig. 15. Comparison of the $p = 2$ Debye-component intensity I_1 with the approximation of Eq. (28) for the TE polarized surface wave and complex ray for $x = 100$ and $n = 1.333$. The approximation of Eq. (28) has been offset by a factor of 100 for clarity.

duced on the other side of the droplet, as shown in Fig. 14, will eventually overtake the complex ray scattered intensity.^{45,46} As a result, an interference pattern will be formed in the angular interval in which these two effects are of comparable strength. This interference in the $p = 2$ Debye intensity corresponding to the S_1 scattering amplitude is shown in Fig. 15. For $\theta \leq 115^\circ$, $\log I_1$ is linear in scattering angle, indicating surface wave dominance, and, for $\theta \geq 115^\circ$, $\log I_1$ falls off faster than linearly in scattering angle, indicating complex ray dominance. Again, to verify this, we compared the intensity of the $p = 2$ term of the Debye series with

$$I_{\text{approximate}}^{p=2}(\theta) = |E_{\text{surface wave}}^{p=2, j=1}(\theta) + E_{\text{Airy}}^{p=2}(\theta)|^2 \quad (28)$$

in Fig. 15. The agreement between Eq. (28) and the Debye series result is quite good, considering that the Airy theory parameterization of Eq. (9) and the surface-wave parameterization of Eq. (21) are expected to be only qualitatively accurate for size parameters as low as $x = 100$.

Since the surface-wave-complex-ray interference structure of Fig. 15 occurs at an intensity level approximately 7 orders of magnitude below the intensity level of the rainbow peak, the effect is not expected to be observable.

8. MEASUREMENT OF SURFACE-WAVE-GEOMETRICAL-RAY INTERFERENCE

An experiment was performed to observe the interference between geometrical rays and the secondary radiation shed by surface waves. The region showing most promise for making this measurement is at scattering angles between 90° and 110° in the vicinity of the second-order rainbow. A focused laser beam was employed, as shown in Fig. 16 and described in Section 5, to increase the visibility of the $p = 3$ rainbow and its supernumeraries and to decrease the background intensity of the light reflected by the droplet.

A focused, linearly polarized beam from a 5-W argon-ion laser ($\lambda = 514.5$ nm) was used to illuminate water droplets that were generated at a rate of 53,240/s by a vibrating orifice droplet generator, as shown in the experimental setup in Fig. 17. The size of the droplets was determined by weighing a sample of the droplets collected over a period of several minutes. Details of this method are given in Ref. 47. Uniform-sized droplets (86.6 ± 1.5 μm) passed through the waist of the laser beam that was measured to be 40 ± 5 μm . A lens with a 25-cm focal length (FL) was found to be ideal for this application for two reasons: (1) it produced a waist that was approximately half the diameter of the droplet, and (2) the length of the waist was long enough to ensure that the rays incident upon the droplet were parallel. If the rays had been converging or diverging, then the positions of the rainbow and its supernumeraries would have been shifted. When a viewing screen was placed beside the droplet stream and parallel to the laser beam, the scattering interval $30^\circ \leq \theta \leq 150^\circ$ could be observed, and the first- and the second-order rainbows were readily evident. By adjusting the droplet stream with a micropositioner so that the laser beam was incident upon either the left- or the right-hand side of the droplet center line, we could make either the first- or the second-order rainbow more intense while the other rainbow was extinguished. When the laser beam was incident near the side of the droplet closest to the screen, thus illuminating the second-order rainbow, the reflected intensity was largely confined to the forward hemisphere and no longer obscured the second-order rainbow supernumeraries. A photograph of the second-order rainbow obtained by using this arrangement is shown in Fig. 18. The photograph was taken by replacing the screen with a film holder.

A frame of Polaroid film was exposed by the scattered light for 0.005 s by using a camera shutter located at the exit port of the laser. To avoid blurring produced by small fluctuations in the droplet stream from air currents in the room, longer exposures using lower-power laser beams were not taken. Moving the droplet generator head close to the laser beam to reduce the effects of the air currents was not practical because the droplets were unstable and not spherical in this region. For the conditions of Fig. 18 the droplet generator head was approximately 5 cm from the laser beam. Note that the figure is ori-

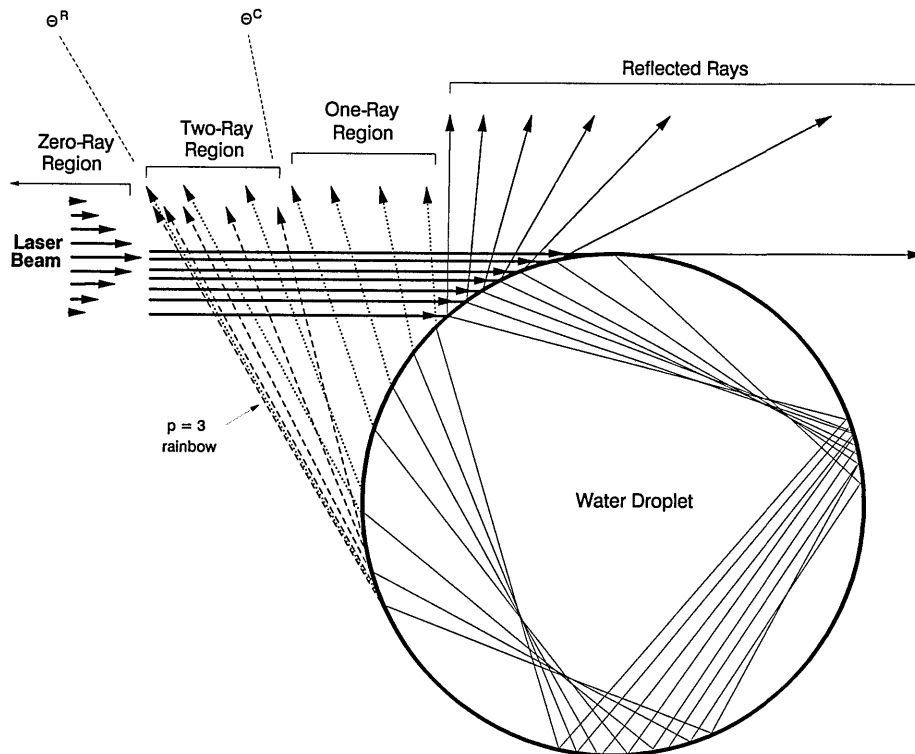


Fig. 16. Laser beam with a small diameter illuminating a water droplet close to one edge. This focused laser beam causes the $p = 3$ rainbow and its supernumeraries to be more intense than other rainbows and confines the reflected rays to the forward-scattering hemisphere.

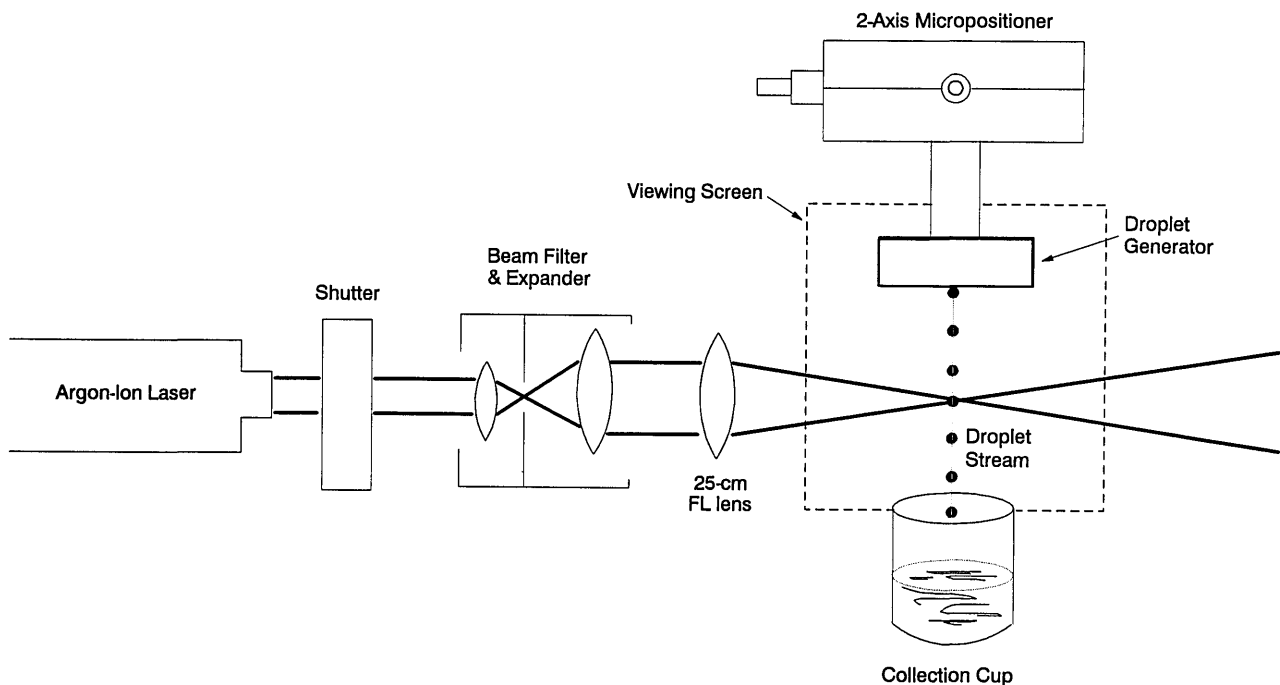


Fig. 17. Experimental apparatus. Light scattered by the droplets in the angular range $30^\circ \leq \theta \leq 150^\circ$ is observed on the viewing screen.

ented so that the scattering pattern is consistent with the orientation of the rays in Figs. 16 and 17; thus the scattering angle in Fig. 18 decreases from left to right. On the left-hand side of Fig. 18 the broad intense region is the $p = 3$ rainbow, with the supernumerary region located to the right of it in the direction of decreasing scattering angle. Farther into the forward-scattering direction the

supernumeraries become washed out by the increasing background of the $p = 0$ reflected light.

After photographing the scattering pattern, we digitized the photograph and compared it with the Debye-series calculation for $p = 3$, as shown in Fig. 19. No compensation for the nonlinearity of the film was made. The abscissa in this figure has two labels: one in mil-

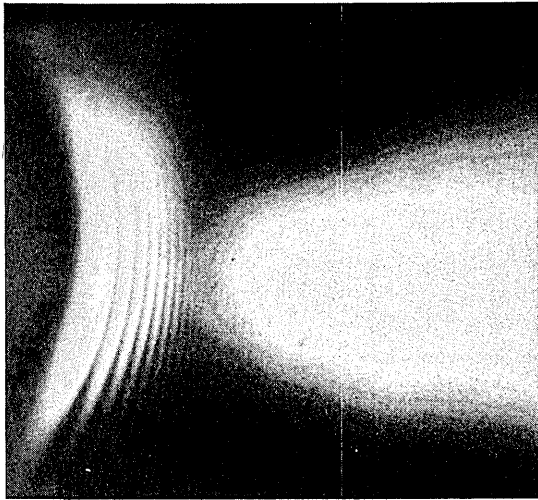


Fig. 18. Scattered light intensity for a 40- μm -diameter laser beam incident near the edge of an 86.6- μm -diameter water droplet. The scattering angle decreases from left to right. The broad illumination on the right-hand side of the photograph is reflection from the droplet. The interference pattern on the left-hand side is the second-order rainbow and its supernumeraries.

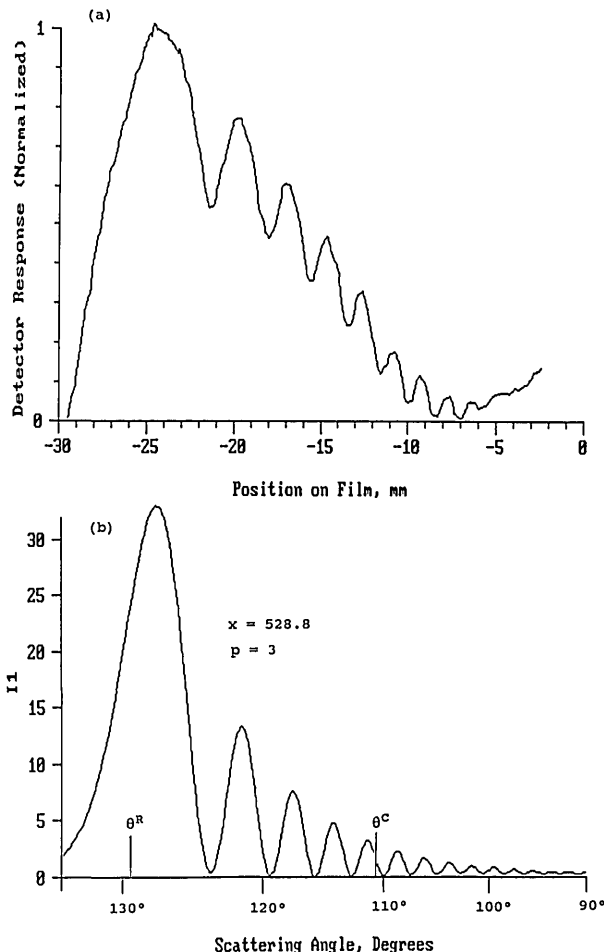


Fig. 19. Comparison between the Debye-component intensity and experiment. (a) Detector response (normalized) as a function of position on the film for the digitization of the photograph of Fig. 18. The four oscillations between -12 and -6 mm on the film ($\theta < \theta^C$) are the geometrical-ray-surface-wave interference. The rise in the detector response at film positions greater than -6 mm ($\theta \leq 100^\circ$) is due to reflection by the droplet surface. (b) $p = 3$ Debye intensity I_1 for $x = 528.8$ and $n = 1.333$ as a function of the scattering angle.

limeters and one in degrees. A scattering angle of 90° corresponds to a position on the film of 0 mm. The degree tick marks are not linear because the film was held with a flat rather than a circular film holder. The experimental data show interference oscillations that begin at the rainbow angle, continue through the two-ray supernumerary region, and extend well into the one-ray region, which begins on the film at the position -12 mm. The positions of these oscillations correspond to the expected positions of the supernumeraries of the second-order rainbow for an $x = 528.8$ sphere as obtained from the $p = 3$ Debye-component intensity. Additional calculations were performed to ascertain that these oscillations were not a result of interference between the one remaining $p = 3$ geometrical ray and the $p = 0$ reflected rays. These calculations showed that such an interference pattern would have had a periodicity greatly different from the one observed. Thus we are confident that the oscillations that were observed in the one-ray region are a result of the interference between the geometrical ray and the secondary radiation shed by the surface waves described in Section 5.

9. CONCLUSIONS

When one thinks about electromagnetic scattering by a dielectric sphere, one's physical picture of the scattering is different from one's mathematical calculation of it. Physically, one thinks of scattering as the resultant sum of a number of mechanisms such as geometrical rays, rainbows, glories, surface waves, and diffraction and the wave interference between them. Mathematically, one calculates the scattering in terms of the effect of the interface between two dielectrics on spherical multipole partial waves and the interference between the partial waves. The difficulty in reconciling these two modes of thought lies in the facts that (1) many partial waves contribute to a single physical mechanism and (2) only a portion of the scattering amplitude for each partial wave contributes to a given mechanism. The connection between the mathematical and the physical modes of thought is expressed in a simple way by the Debye series. We hope to have demonstrated the simplicity and the power of this connection.

The Debye series also makes evident one other feature of electromagnetic scattering that is not evident in the geometrical model of scattering, namely, that the scattered intensity as a function of scattering angle is smoothly varying. Ray theory permits (in fact demands) discontinuities both in the scattered intensity as a function of scattering angle and in the derivative of the intensity. The discontinuity in the intensity occurs at the two-ray-zero-ray transition at the rainbow scattering angle. The discontinuity in the derivative of the intensity occurs at the one-ray-zero-ray transition at the critical scattering angle of the grazing-incident ray. Wave theory smooths these discontinuities by the action of the complex ray at the two-ray-zero-ray transition and the secondary radiation shed by surface waves at the one-ray-zero-ray transition. These physical mechanisms that implement the smoothing of the scattered intensity at the more-rays-fewer-rays transitions produce new features in the scattering as well. They interfere with each other and with

geometrical rays, giving additional structure to the scattered intensity. Under favorable circumstances, at least one of these new structures, the geometrical-ray-surface-wave interference, is observable in laser light scattering.

APPENDIX A: DERIVATION OF THE DEBYE SERIES

Consider monochromatic TE and TM spherical multipole waves in a medium whose refractive index is n . The time dependence of the waves is taken to be $\exp(-i\omega t)$. The electric and the magnetic fields of the spherical waves are derived from a scalar potential $\psi(\mathbf{r}, \theta, \phi)$ that satisfies the wave equation

$$\nabla^2 \psi + n^2 k^2 \psi = 0, \quad (\text{A1})$$

where

$$k = \frac{\omega}{c}. \quad (\text{A2})$$

The fields are

$$\begin{aligned} \mathbf{E} &= -\mathbf{r} \times \nabla \psi, \\ \mathbf{B} &= \frac{-i}{\omega} \nabla \times \mathbf{E} \end{aligned} \quad (\text{A3})$$

for the TE spherical multipole waves, and they are

$$\begin{aligned} \mathbf{E} &= \frac{i}{\omega} \frac{c^2}{n^2} \nabla \times \mathbf{B}, \\ \mathbf{B} &= \frac{n}{c} \mathbf{r} \times \nabla \psi \end{aligned} \quad (\text{A4})$$

for TM spherical multipole waves. The solutions to scalar wave equation (A1) are

$$\psi(r, \theta, \phi) = \sum_{lm} A_{lm} \left\{ \frac{j_l(nkr)}{n_l(nkr)} \right\} P_l^m(\cos \theta) \begin{Bmatrix} \cos m\phi \\ \sin m\phi \end{Bmatrix}, \quad (\text{A5})$$

where j_l and n_l are spherical Bessel functions and spherical Neumann functions, respectively (also known as spherical Bessel functions of the first and the second kinds), and P_l^m are the associated Legendre polynomials. We adopt the sign convention for the spherical Bessel and Neumann functions,

$$\begin{aligned} j_0(nkr) &= \frac{\sin(nkr)}{nkr}, \\ n_0(nkr) &= \frac{-\cos(nkr)}{nkr}. \end{aligned} \quad (\text{A6})$$

With this sign convention, the Wronskian relation for the spherical Bessel and Neumann functions is

$$j_l(nkr)n_l'(nkr) - j_l'(nkr)n_l(nkr) = (nkr)^{-2}, \quad (\text{A7})$$

where the prime indicates the derivative of a function with respect to its argument. The solutions of Eq. (A5) represent standing waves. When considering outgoing and incoming traveling waves, we employ spherical Hankel functions of the first and the second kinds:

$$\begin{aligned} h_l^{(1)}(nkr) &= j_l(nkr) + in_l(nkr), \\ h_l^{(2)}(nkr) &= j_l(nkr) - in_l(nkr), \end{aligned} \quad (\text{A8})$$

respectively.

Consider a dielectric sphere whose radius is a and whose refractive index is n_1 (region 1) embedded in another dielectric material whose refractive index is n_2 (region 2). The center of the sphere is taken to be at the origin of the coordinates. If a spherical multipole wave propagates from one region to another, the tangential components of its electric and magnetic fields must be continuous at the interface. For TE waves this continuity of the field components requires that

$$\frac{\Psi(x)}{n_2} = \frac{\Psi(y)}{n_1}, \quad (\text{A9})$$

$$\Psi'(x) = \Psi'(y), \quad (\text{A10})$$

where

$$\begin{aligned} x &= n_2 ka, \\ y &= n_1 ka, \end{aligned} \quad (\text{A11})$$

$$\Psi(nkr) \equiv nkr\psi(nkr). \quad (\text{A12})$$

For TM waves the continuity of the field components requires that

$$\Psi(x) = \Psi(y), \quad (\text{A13})$$

$$\frac{\Psi'(x)}{n_2} = \frac{\Psi'(y)}{n_1}. \quad (\text{A14})$$

Consider the single incoming TE or TM spherical multipole wave in region 2,

$$\Psi = H_l^{(2)}(n_2 kr) P_l^m(\cos \theta) \begin{Bmatrix} \cos m\phi \\ \sin m\phi \end{Bmatrix}, \quad (\text{A15})$$

where

$$H_l^{(2)}(n_2 kr) \equiv n_2 kr h_l^{(2)}(nkr). \quad (\text{A16})$$

When this spherically incoming wave encounters the interface at $r = a$, a portion of it, T_l^{21} , is transmitted into the sphere, and another portion, R_l^{22} , is reflected back into region 2. The complete TE or TM multipole wave in the two regions is then

$$\begin{aligned} \Psi_1 &= T_l^{21} H_l^{(2)}(n_1 kr) P_l^m(\cos \theta) \begin{Bmatrix} \cos m\phi \\ \sin m\phi \end{Bmatrix} \quad \text{for } r \leq a, \\ \Psi_2 &= [H_l^{(2)}(n_2 kr) + R_l^{22} H_l^{(1)}(n_2 kr)] \\ &\quad \times P_l^m(\cos \theta) \begin{Bmatrix} \cos m\phi \\ \sin m\phi \end{Bmatrix} \quad \text{for } r \geq a. \end{aligned} \quad (\text{A17})$$

Applying the boundary conditions [Eqs. (A9) and (A10) or (A13) and (A14)] yields two linear equations in the two unknowns, T_l^{21} and R_l^{22} . The solutions of these equations are

$$T_l^{21} = -\left(\frac{n_1}{n_2}\right) \frac{2i}{D}, \quad (\text{A18})$$

$$R_l^{22} = \frac{[\alpha H_l^{(2)'}(x) H_l^{(2)}(y) - \beta H_l^{(2)}(x) H_l^{(2)'}(y)]}{D}, \quad (\text{A19})$$

where

$$\alpha = \begin{cases} 1 & \text{for TE spherical multipole waves} \\ n_1/n_2 & \text{for TM spherical multipole waves} \end{cases}, \quad (\text{A20})$$

$$\beta = \begin{cases} n_1/n_2 & \text{for TE spherical multipole waves} \\ 1 & \text{for TM spherical multipole waves} \end{cases}, \quad (\text{A21})$$

$$D = -\alpha H_l^{(1)'}(x) H_l^{(2)}(y) + \beta H_l^{(1)}(x) H_l^{(2)'}(y), \quad (\text{A22})$$

and Eq. (A7) has been used to simplify the expression for T_l^{21} .

Consider now the single outgoing TE or TM spherical multipole wave in region 1,

$$\Psi = H_l^{(1)}(n_1 k r) P_l^m(\cos \theta) \begin{cases} \cos m\phi \\ \sin m\phi \end{cases}. \quad (\text{A23})$$

When this spherically outgoing wave encounters the interface at $r = a$, a portion of it, T_l^{12} , is transmitted out of the sphere, and another portion, R_l^{11} , is reflected back into it. The complete TE or TM multipole wave in the two regions is then

$$\begin{aligned} \Psi_1 &= [H_l^{(1)}(n_1 k r) + R_l^{11} H_l^{(2)}(n_1 k r)] P_l^m(\cos \theta) \begin{cases} \cos m\phi \\ \sin m\phi \end{cases} \\ &\quad \text{for } r \leq a, \\ \Psi_2 &= T_l^{12} H_l^{(1)}(n_2 k r) P_l^m(\cos \theta) \begin{cases} \cos m\phi \\ \sin m\phi \end{cases} \\ &\quad \text{for } r \geq a. \end{aligned} \quad (\text{A24})$$

Applying the boundary conditions [Eqs. (A9) and (A10) or (A13) and (A14)] again yields two linear equations in the two unknowns T_l^{12} and R_l^{11} . The solutions of these equations are

$$T_l^{12} = -2i/D, \quad (\text{A25})$$

$$R_l^{11} = \frac{[\alpha H_l^{(1)'}(x) H_l^{(1)}(y) - \beta H_l^{(1)}(x) H_l^{(1)'}(y)]}{D}. \quad (\text{A26})$$

Equations (A18)–(A22), (A25), and (A26) are identical to Eqs. (2.11), (2.13), and (2.15)–(2.18) of Ref. 8 except that the right-hand sides of Eqs. (2.17) and (2.18) of that reference should be multiplied by nx^2 .

Consider the quantity $(1 - R_l^{11})(1 - R_l^{22}) - T_l^{21} T_l^{12}$ for either the TE or the TM spherical multipole waves. Substituting Eqs. (A19) and (A26) and using the expressions for T_l^{21} and T_l^{12} before the simplifications provided by the Wronskian relation, we find the quantity to factor, after much algebra, into

$$(1 - R_l^{11})(1 - R_l^{22}) - T_l^{21} T_l^{12} = \frac{4[-\alpha J_l'(x) J_l(y) + \beta J_l(x) J_l'(y)]}{D}, \quad (\text{A27})$$

where

$$J_l(nkr) \equiv nkr j_l(nkr). \quad (\text{A28})$$

Dividing Eq. (A27) by $(1 - R_l^{11})$, we obtain

$$\begin{aligned} &\frac{-\alpha J_l'(x) J_l(y) + \beta J_l(x) J_l'(y)}{-\alpha H_l^{(1)'}(x) J_l(y) + \beta H_l^{(1)}(x) J_l'(y)} \\ &= \frac{1}{2} \left[1 - R_l^{22} - \frac{T_l^{21} T_l^{12}}{1 - R_l^{11}} \right] \\ &= \frac{1}{2} \left[1 - R_l^{22} - \sum_{p=1}^{\infty} T_l^{21} (R_l^{11})^{p-1} T_l^{12} \right]. \end{aligned} \quad (\text{A29})$$

The left-hand side of Eq. (A29) is recognized as the Mie far-field partial-wave scattering amplitudes a_l (TM amplitude) and b_l (TE amplitude). The Mie-scattered electric field is written in terms of the a_l and the b_l partial-wave amplitudes as

$$\begin{aligned} \mathbf{E}(R, \theta, \phi) &= \frac{E_0 a}{R x} \exp(ikR) \\ &\quad \times [-iS_2(\theta) \cos \phi \hat{u}_\theta + iS_1(\theta) \sin \phi \hat{u}_\phi] \end{aligned} \quad (\text{A30})$$

for an incident electric field in the \hat{u}_x direction, where

$$S_1(\theta) = \sum_{l=1}^{l_{\max}} \frac{2l+1}{l(l+1)} [a_l \pi_l(\theta) + b_l \tau_l(\theta)], \quad (\text{A31})$$

$$S_2(\theta) = \sum_{l=1}^{l_{\max}} \frac{2l+1}{l(l+1)} [a_l \tau_l(\theta) + b_l \pi_l(\theta)], \quad (\text{A32})$$

$$\pi_l(\theta) = \frac{1}{\sin \theta} P_l^1(\theta), \quad (\text{A33})$$

$$\tau_l(\theta) = \frac{d}{d\theta} P_l^1(\theta), \quad (\text{A34})$$

$$l_{\max} = x + 4.05x^{1/3} + 2. \quad (\text{A35})$$

Also,

$$I_1(\theta) = |S_1(\theta)|^2, \quad (\text{A36})$$

$$I_2(\theta) = |S_2(\theta)|^2. \quad (\text{A37})$$

For a large sphere $x \gg 1$, large partial waves $l \gg 1$, and θ away from 0° and 180° , the angular function $\pi_l(\theta)$ is small in comparison with $\tau_l(\theta)$.⁴⁸ In this limit, the scattering amplitude S_1 becomes associated with the TE spherical multipole waves and the TE polarized geometrical rays, while the scattering amplitude S_2 becomes associated with the TM spherical multipole waves and the TM polarized geometrical rays.

The right-hand side of Eq. (A29) is the Debye-series expansion of the partial-wave scattering amplitudes. The various terms of the right-hand side of Eq. (A29) have simple physical interpretations. The first term, $\frac{1}{2}[1]$, when inserted for a_l and b_l in the expressions for the Mie electric field and summed over l , describes the diffraction of the incident plane wave around the sphere.⁴⁹

The second term, $\frac{1}{2}[-R_l^{22}]$, when inserted for a_l and b_l and summed over l , represents the outgoing spherical multipole waves that have reflected from the surface of the sphere. The diffraction and the reflection terms, when taken separately, do not approach zero as l goes to infinity (and thus the sums over l go to infinity). However, if the two terms are added together and then summed over l they do approach zero, which leads to a finite sum over l .³¹ Thus in its present form the Debye series is not amenable to separation of the diffraction term from the reflection term. Previous calculations in which the diffraction term was summed separately from the reflection term^{49,50} were made by truncating the sum over l at $l = x$. Truncation in this manner is an approximation and is accurate only for large values of x . Truncation of the diffraction term of the Debye series at $l = x$ has been shown to be equivalent to Fraunhofer diffraction by a circular aperture of radius a . We conjecture that the separate divergences of the diffraction and the $p = 0$ terms of the Debye series are artificial in that they result from the infinite extent of the incident plane wave.

The third term of Eq. (A29) is an infinite sum that describes a geometrical series. The individual terms of the

series represent light that has penetrated the sphere, undergone $p - 1$ internal reflections, and then emerged from the sphere. For example, when the $p = 2$ contribution to the Debye series is calculated, the appropriate term in the sum that describes a_l and b_l is $-\frac{1}{2}[T_l^{21}R_l^{11}T_l^{12}]$. This represents the spherical waves that were transmitted into the sphere $[T_l^{21}]$, propagated radially inward toward the center of the sphere, passed through it, propagated radially outward, reflected off the inner surface of the sphere $[R_l^{11}]$, propagated inward toward the center and back out a second time, and finally transmitted out of the sphere $[T_l^{12}]$ and propagated into the far field.

If all the Debye-series terms are first added together and then summed over l , the results are identical to those from Mie scattering. In this sense, Eq. (A29) interprets the Mie partial-wave scattering amplitudes as the composite result of a multiple-scattering process.

REFERENCES

1. H. C. van de Hulst, *Light Scattering by Small Particles* (Dover, New York, 1957), Chap. 9.
2. M. Kerker, *The Scattering of Light and Other Electromagnetic Radiation* (Academic, New York, 1969), Chap. 3.
3. C. F. Bohren and D. R. Huffman, *Absorption and Scattering of Light by Small Particles* (Wiley-Interscience, New York, 1983), Chap. 4.
4. B. Van der Pol and H. Bremmer, "The diffraction of electromagnetic waves from an electrical point source round a finitely conducting sphere, with applications to radiotelegraphy and the theory of the rainbow," *Philos. Mag.* **24**, 141–176, 825–864 (1937).
5. H. M. Nussenzveig, "High-frequency scattering by a transparent sphere. I. Direct reflection and transmission," *J. Math. Phys.* **10**, 82–124 (1969).
6. H. M. Nussenzveig, "High-frequency scattering by a transparent sphere II. Theory of the rainbow and the glory," *J. Math. Phys.* **10**, 125–176 (1969).
7. V. Khare, "Short-wavelength scattering of electromagnetic waves by a homogeneous dielectric sphere," Ph.D. dissertation (University of Rochester, Rochester, N.Y., 1976).
8. J. A. Lock, "Cooperative effects among partial waves in Mie scattering," *J. Opt. Soc. Am. A* **5**, 2032–2044 (1988).
9. J. A. Lock and E. A. Hovenac, "Internal caustic structure of illuminated liquid droplets," *J. Opt. Soc. Am. A* **8**, 1541–1552 (1991).
10. A. Ungut, G. Grehan, and G. Gouesbet, "Comparisons between geometrical optics and Lorenz-Mie theory," *Appl. Opt.* **20**, 2911–2918 (1981).
11. J. D. Walker, "Multiple rainbows from single drops of water and other liquids," *Am. J. Phys.* **44**, 421–433 (1976).
12. J. D. Walker, "Mysteries of rainbows, notably their rare supernumerary arcs," *Sci. Am.* **242**(6), 174–184 (1980).
13. J. B. Keller, "A geometrical theory of diffraction," in *Calculus of Variations and Its Applications: Proceedings of the Symposium in Applied Mathematics*, L. M. Graves, ed. (McGraw-Hill, New York, 1958), Vol. VIII, pp. 27–52.
14. V. Khare and H. M. Nussenzveig, "Theory of the rainbow," *Phys. Rev. Lett.* **33**, 976–980 (1974).
15. H. M. Nussenzveig, "Complex angular momentum theory of the rainbow and the glory," *J. Opt. Soc. Am.* **69**, 1068–1079, 1193–1194 (1979).
16. B. R. Levy and J. B. Keller, "Diffraction by a smooth object," *Commun. Pure Appl. Math.* **12**, 159–209 (1959).
17. S. I. Rubinow, "Scattering from a penetrable sphere at short wavelengths," *Ann. Phys. (N.Y.)* **14**, 305–332 (1961).
18. H. M. Nussenzveig, "High-frequency scattering by an impenetrable sphere," *Ann. Phys. (N.Y.)* **34**, 23–95 (1965).
19. V. Khare and H. M. Nussenzveig, "Theory of the glory," *Phys. Rev. Lett.* **38**, 1279–1282 (1977).
20. V. Khare and H. M. Nussenzveig, "Theory of the glory," in *Statistical Mechanics and Statistical Methods in Theory and Application*, U. Landman, ed. (Plenum, New York, 1976), pp. 723–764.
21. M. V. Berry, J. F. Nye, and F. J. Wright, "The elliptic umbilic diffraction catastrophe," *Philos. Trans. R. Soc. London* **291**, 453–484 (1979), App. C.
22. F. J. Wright, "The Stokes set of the cusp diffraction catastrophe," *J. Phys. A* **13**, 2913–2928 (1980).
23. M. V. Berry and C. Upstill, "Catastrophe optics: morphologies of caustics and their diffraction patterns," *Prog. Opt.* **18**, 257–346 (1980), Sec. 3.3.ii.
24. M. V. Berry and C. J. Howls, "Stokes surfaces of diffraction catastrophes with codimension three," *Nonlinearity* **3**, 281–291 (1990).
25. C. K. Frederickson and P. L. Marston, "Transverse cusp diffraction catastrophes produced by reflecting ultrasonic tone bursts from curved surfaces," in *Proceedings of the IUTAM Symposium of Elastic Wave Propagation and Ultrasonic Nondestructive Evaluation*, S. K. Datta, J. D. Achenbach, and Y. D. S. Rajapakse, eds. (Elsevier, Amsterdam, 1989).
26. K. W. Ford and J. A. Wheeler, "Semiclassical description of scattering," *Ann. Phys. (N.Y.)* **7**, 259–286 (1959).
27. J. R. Reitz, F. J. Milford, and R. W. Christy, *Foundations of Electromagnetic Theory*, 3rd ed. (Addison-Wesley, Reading, Mass., 1979), Sec. 18.2.
28. Ref. 1, Sec. 12.22.
29. Ref. 1, Sec. 12.34.
30. H. C. van de Hulst, "A theory of the anti-corona," *J. Opt. Soc. Am.* **37**, 16–22 (1947).
31. M. V. Berry, "Uniform approximation for glory scattering and diffraction peaks," *J. Phys. B* **2**, 381–392 (1969).
32. M. V. Berry, "Waves and Thom's theorem," *Adv. Phys.* **25**, 1–26 (1976).
33. H. M. Nussenzveig and W. Wiscombe, "Forward optical glory," *Opt. Lett.* **5**, 455–457 (1980).
34. W. J. Humphreys, *Physics of the Air* (Dover, New York, 1964), Chap. 3.
35. R. T. Wang and H. C. van de Hulst, "Rainbows: Mie computations and the Airy approximation," *Appl. Opt.* **30**, 106–117 (1991).
36. M. Abramowitz and I. A. Stegun, eds., *Handbook of Mathematical Functions* (National Bureau of Standards, Washington, D.C., 1964), Sec. 10.4.
37. C. W. Querfeld, "Mie atmospheric optics," *J. Opt. Soc. Am.* **55**, 105–106 (1965).
38. K. Sassen, "Angular scattering and rainbow formation in pendant drops," *J. Opt. Soc. Am.* **69**, 1083–1089 (1979).
39. G. P. Können and J. H. de Boer, "Polarized rainbow," *Appl. Opt.* **18**, 1961–1965 (1979).
40. Ref. 1, Sec. 12.31.
41. Ref. 1, Sec. 17.31.
42. K. L. Williams and P. L. Marston, "Backscattering from an elastic sphere: Sommerfeld-Watson transformation and experimental confirmation," *J. Acoust. Soc. Am.* **78**, 1093–1102 (1985).
43. E. DiSalvo and G. A. Viano, "Surface waves in pion-proton elastic scattering," *Nuovo Cimento A* **59**, 11–37 (1980).
44. E. Heyman and L. B. Felson, "High frequency fields in the presence of a curved dielectric interface," *IEEE Trans. Antennas Propag.* **AP32**, 969–978 (1984).
45. Ref. 6, p. 142.
46. H. M. Nussenzveig, "Applications of Regge poles to short-wavelength scattering," in J. E. Bowcock, ed., *Methods and Problems of Theoretical Physics* (North-Holland, Amsterdam, 1970), p. 225.
47. E. A. Hovenac, "Droplet sizing instrumentation used for icing research: operation, calibration, and accuracy," NASA CR-182293 DOT/FAA/CD-89/13 (NASA Lewis Research Center, Cleveland, Ohio, 1989).
48. Ref. 1, Sec. 12.33.
49. Ref. 1, Sec. 12.32.
50. J. A. Lock and L. Yang, "Interference between diffraction and transmission in the Mie extinction efficiency," *J. Opt. Soc. Am. A* **8**, 1132–1134 (1991).